Drew University

College of Liberal Arts

Developing a LRRK2 Model of Parkinson's Disease in *C. elegans*

A Thesis in Neuroscience

By

Evan Fairweather

Submitted in Partial Fulfillment

Of the Requirements for the Degree of

Bachelor of Science

With Specialized Honors in Neuroscience

May 2022

Abstract

Parkinson's disease (PD) is the second most common neurodegenerative disorder worldwide. PD has a multifactorial etiology, with genetic, environmental, and lifestyle factors identified by epidemiological studies. One such genetic factor is mutation of the leucine-rich-repeat-kinase-2 gene (LRRK2), responsible for up to 40% of familial PD in certain populations. While treatment options such as pharmacological dopamine supplementation with L-DOPA are available, they do not address the underlying molecular mechanisms of disease. As such, the identification of targeted therapeutic compounds stands to significantly reduce the morbidity of Parkinson's disease. The development of a model system using the nematode *C. elegans* is the first step in such a process. With a simple, well characterized nervous system with significant biochemical similarity to that of humans, they have demonstrated considerable utility in modeling the mechanisms of human neurological disease. This study sought to develop a robust behavioral assay capable of quantifying *C. elegans* motor deficits, as well as correlate such deficits with the degeneration of cephalic dopaminergic neurons. Such a model system could then be employed in the screening of novel therapeutics, such as kinase inhibitors for the treatment of LRRK2-PD. It was found that the basal slowing assay, which measures the change in locomotor rate in the presence and absence of a bacterial lawn, may have potential for such purposes. As hypothesized, wildtype worms exhibited an intact basal slowing response, whereas dopamine deficient transgenic worms exhibited a phenotype consistent with the loss of this dopaminergic behavior. However, observations of LRRK2 mutant *C. elegans* were inconsistent with expectations, wherein no time-dependent loss of the basal slowing response was observed despite gradual degeneration of their dopaminergic neurons. Further study is needed to evaluate the utility and practicality of this assay in the development of a robust PD model system.

TABLE OF CONTENTS

Contents

Introduction

Parkinson's Disease: Presentation, Diagnosis, & Epidemiology

Penned by James Parkinson in 1817, "An essay on the Shaking Palsy" was the first publication to describe the progressive neurodegenerative disorder we know today as Parkinson's disease (PD) (Simon et al. 2020). In the centuries since its discovery, great strides have been made in our understanding of the mechanisms underlying the disease. Thanks to advances in biomedical research, treatments exist to relieve symptoms and improve quality of life (Poewe et al. 2017). However, no definitive cure exists. With substantial growth in PD prevalence projected over the coming decades, the development of novel therapeutics has become an important area of biomedical research.

PD is the second most common neurodegenerative disorder, with Alzheimer's disease being the first (Cooper and Van Raamsdonk 2018). It affects over 10 million patients worldwide. Epidemiologists report that the incidence rate of Parkinson's disease ranges between 5 and 35 new cases per 100,000 people (Cooper and Van Raamsdonk 2018; Simon et al. 2020). This variability is due to demographic, environmental, and genetic factors that influence one's susceptibility. Age is a significant factor, as one's risk for developing PD increases 5 to 10-fold between age 60 and 90 (Poewe et al. 2017; Simon et al. 2020). The global prevalence rate is estimated to be around 0.3%, though this exceeds 3% when the population is restricted to individuals 80 and older. Due to the world's aging population, the prevalence of PD is forecasted to double within the next 20 years. With this will come a substantial increase in its economic and social impacts.

There are 4 main features of Parkinson's disease that are considered when making a diagnosis: tremor at rest, muscle rigidity, akinesia (bradykinesia) and postural instability (Jankovic 2007). Akinesia (bradykinesia) or slowed movement with a loss of fine motor control, is the most characteristic clinical feature that appears due to deficits in planning, initiating, and executing voluntary movements. Postural instability, the final of these 4 cardinal symptoms, is typically a late manifestation. Non-motor symptoms can also be observed, including a sixfold increase in dementia risk (Jankovic 2007). Other neuropsychiatric manifestations include obsessive-compulsive and impulsive behaviors due to dysregulation of certain dopaminergic circuits. Depression and sleep disruptions are also possible (Simon et al. 2020). Progression of the disease is highly variable, with the severity of symptoms and degree of disability increasing over time in a non-linear fashion (Jankovic 2007). The age of symptom onset is typically in the late 50s, though this ranges significantly (Poewe et al. 2017).

Diagnosis of PD is made based on the patient's history and clinical examination findings (Jankovic 2007). At the present time there is no test available to conclusively diagnose PD in a living patient. As such, a diagnosis can only be confirmed by examining the brain for characteristic pathology after death. The presumptive diagnosis of PD is based on the presence of cardinal signs and symptoms (tremor, akinesia, etc.), the patient's past medical and family history, and symptom improvement with dopamine supplementation therapy.

Parkinson's Disease: Dopamine Signaling & Pathophysiology

Before exploring the mechanisms underlying the pathogenesis of Parkinson's disease, it is helpful to understand the basics of dopamine signaling within the brain. Dopamine is a neurotransmitter, a signaling molecule released from one neuron, across the synaptic cleft, onto another. It acts as a neuromodulator, altering the responses of target neurons to other

neurotransmitters (Girault and Greengard 2004). This activity is exerted via metabotropic dopamine receptors, which rather than directly opening or closing ion channels, initiate signaling cascades with wide-ranging effects on cellular function. These D1 and D2 dopamine receptors are present in large numbers in the neostriatum, the brain structure encompassing the caudate nucleus, putamen, and nucleus accumbens (fig. 1a). The striatum encompasses just the caudate nucleus and putamen, which are of particular interest to the study of PD since they are components of the basal ganglia. This is the group of subcortical structures (caudate nucleus, putamen, globus pallidus, subthalamic nucleus, and substantia nigra) involved in motor regulation. The brain structure at the center of Parkinson's pathogenesis is the substantia nigra, a collection of dopaminergic neurons in the midbrain. It projects to and provides dopaminergic input to the striatum, facilitating the execution of motor commands. The death of these neurons leads to dysregulation of the basal ganglia's circuitry, thereby leading to the development of symptomatic PD. These neurons are particularly susceptible to damage due to their numerous synapses and long lengths of unmyelinated axons (Poewe et al. 2017).

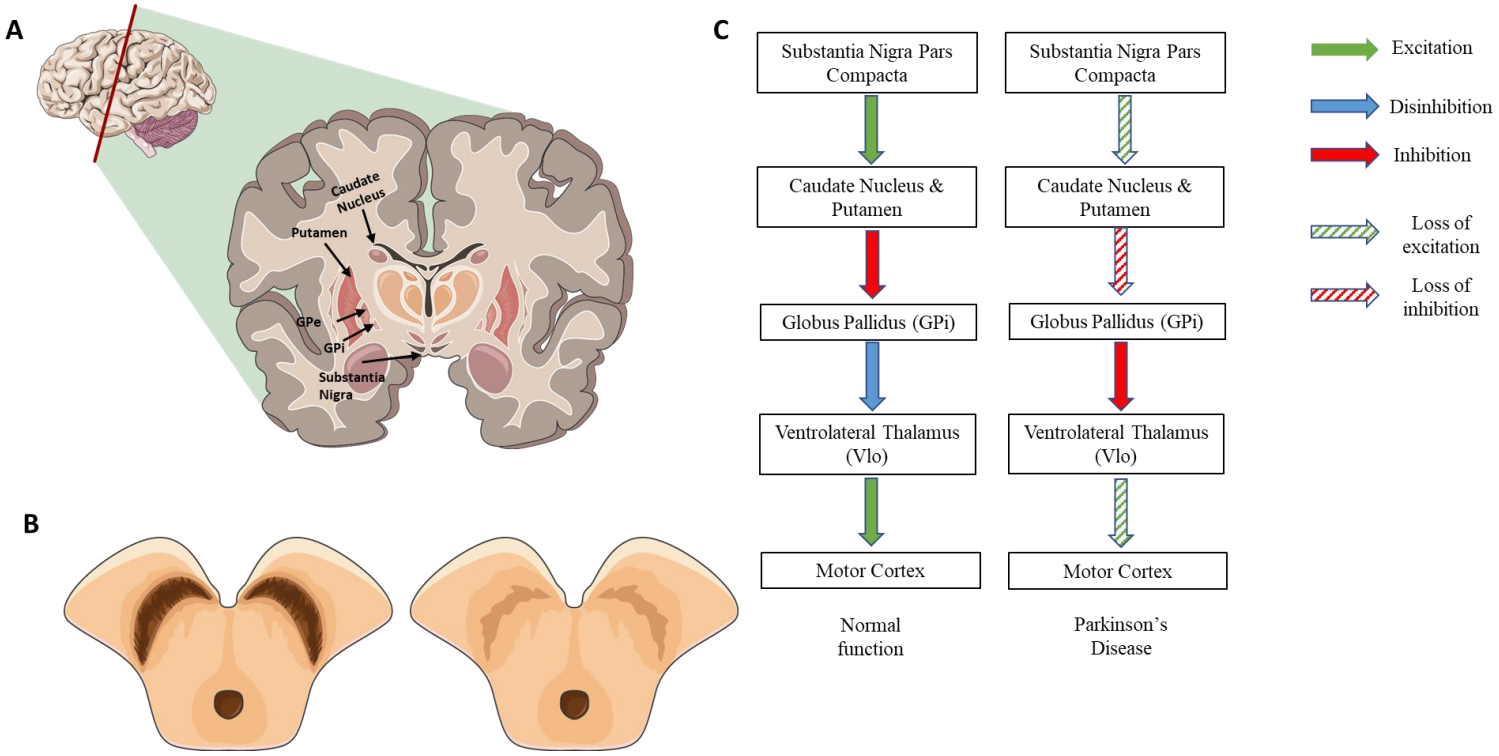

Figure 1. Basal ganglia anatomy and physiology. (A) The basal ganglia consist of several subcortical nuclei responsible for executing motor commands, including the caudate nucleus and putamen (together composing the striatum), globus pallidus, and substantia nigra. (B) Comparison of normal (left) and parkinsonian (right) substantia nigra reveals evidence of neuronal loss. (C). Normally, inhibition of the globus pallidus by the striatum disinhibits the ventrolateral thalamus, permitting the completion of motor actions. Destruction of the substantia nigra leads to a loss of excitation in the striatum, which is no longer able to inhibit the globus pallidus. This leads to continued inhibition of the ventrolateral thalamus and blocking of motor command output to the motor cortex.

Adapted from Lanciego et al. 2012 and Servier Medical Art

Understanding the pathophysiology underlying Parkinson's disease necessitates understanding the normal function of the basal ganglia in motor control. PD primarily concerns the direct pathway, which enables execution of motor commands via thalamocortical disinhibition. This pathway is outlined in figure 1. The substantia nigra pars compacta, a dopaminergic midbrain nucleus, projects to and releases dopamine upon the striatum. This stimulation of the striatum in turn leads to inhibition of the internal segment of the globus pallidus (GPi), which disinhibits the ventrolateral thalamus (VLo) (Lanciego et al. 2012). The ventrolateral thalamus projects to the frontal cortex, which projects to primary and supplementary motor areas of the cerebral cortex. Parkinson's disease is the result of the loss of dopaminergic neurons in the substantia nigra pars compacta (SNpc) (Simon et al. 2020). This deprives the striatum of stimulation, rendering it unable to inhibit the globus pallidus, thereby enabling the GPi to tonically inhibit the activity of VLo. To summarize, death of these dopamine producing neurons reduces dopaminergic input to the direct pathway, thereby disrupting the initiation and termination of motor movements. The loss of cell bodies in the substantia nigra begins well before symptoms become apparent, with some suggesting that around 50% of neurons have been lost by this point (Poewe et al. 2017).

The accumulation of Lewy bodies is often a significant contributor to the death of neurons in the substantia nigra, and such pathology is seen in the brains of all PD patients (Simon et al. 2020). These deposits are composed of α-synuclein, neurofilaments, lipids, and other membrane materials (Maulik et al. 2017). The primary component, α-synuclein, as a highly soluble, presynaptic cytoplasmic protein that is found in the brain, heart, and muscle. Forming in the cytoplasm of affected neurons, these Lewy bodies exert their neurotoxic effects through several pathways (Poewe et al. 2017). It has been suggested that in the earliest stages of PD

pathogenesis, accumulation begins in the dorsal motor nucleus of the vagus nerve (Simon et al. 2020). It then spreads along neural pathways, reaching the substantia nigra. While this model, termed Braak staging, is not observed in 100% of patients, it is generally accepted that α-synuclein accumulation and its associated neurodegenerative effects grow and spread over time.

Consistent with this model, mutations of the gene encoding α-synuclein (SNCA), are implicated in familial PD (Poewe et al. 2017). Single nucleotide polymorphisms at certain loci within this gene have also been linked to an increase in one's risk for developing sporadic PD. The normal function of α-synuclein is yet to be elucidated, though it is suggested to be involved in mitochondrial function, intracellular trafficking, and synaptic vesicles. It becomes neurotoxic through aggregation, where α-synuclein monomers polymerize into insoluble fibrils (Poewe et al. 2017). This process may be accelerated by certain mutations that influence protein misfolding, an overabundance of α-synuclein, or age-related decline in proteolytic mechanisms. The clearance of this α-synuclein is the responsibility of the ubiquitin-protease system and the lysosomal autophagy system (LAS) (Poewe et al. 2017). Both exhibit significant decreases in function with age, thereby increasing one's PD risk.

Pathogenesis is the result of a combination of genetic and environmental factors (Liu et al. 2011; Simon et al. 2020). Though PD is discussed as being either familial or sporadic, it has a multifactorial etiology. As such, that the interaction of various determinants including toxic exposure, trauma, and lifestyle affect one's risk (Simon et al. 2020). These complex relationships are summarized in figure 2, wherein numerous factors including age, decline in cellular debris clearance mechanisms, mitochondrial dysfunction, and environmental exposures contribute to neurotoxicity. This ensuing neuronal death leads to an eventual loss of nigrostriatal dopamine signaling and the symptoms of PD.

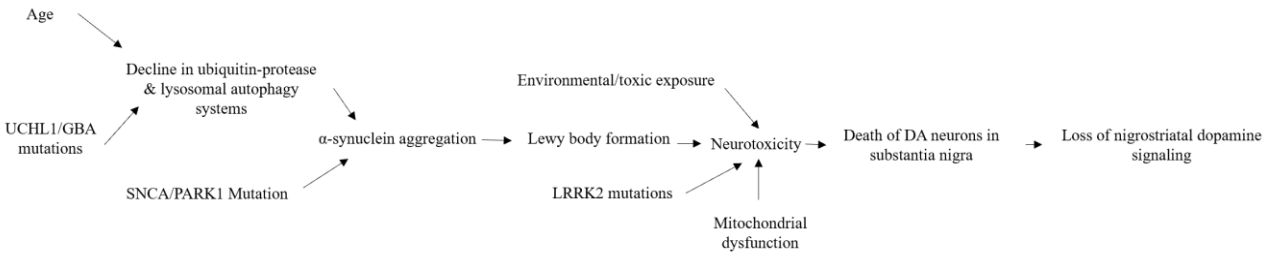

Figure 2. The multifactorial etiology of Parkinson's Disease

Certain identifiable mutations have been associated with 5-10% of cases, though research suggests that genetics are a more minor contributor to PD (Simon et al. 2020). Others suggest that around 15% of cases are familial in nature (Cooper and Van Raamsdonk 2018). Genome wide association studies have implicated genes normally involved in α-synuclein processing, mitochondrial function, oxidative stress, calcium homeostasis, axonal transport, and neuroinflammation (Poewe et al. 2017). There is high variability in the heritability, as well as penetrance, of these mutations. One study, examining nearly 20,000 members of the National Academy of Sciences Twin Registry found a higher concordance of PD in monozygotic twins than dizygotic twins when the age of PD onset was less than 50 years (Goldman et al. 2019). This association became less significant as the age of onset increased beyond 50, indicating a shift in the contributing factors. Genome-wide association studies have estimated the overall heritability of PD to be 27%, while the Swedish Twin Registry reports an average heritability of approximately 34% (Goldman et al. 2019). When the dataset was restricted to twins diagnosed under the age of 50, the heritability of PD jumped to 83%. This decreased to only 19% when the age of diagnosis was greater than 50. These findings suggest that there is a larger genetic component to early onset PD, while environment and lifestyle play a greater role in later onset PD. However, it is important to remember that the development of PD is the result of the interaction of many risk factors. With high variability in the penetrance of these mutations

(Simon et al. 2020). The first gene implicated in PD was SNCA/PARK1, which encodes α-synuclein (Cooper and Van Raamsdonk 2018). Subsequent findings indicated that mutations in the genes PARK4, PARK8, and LRRK2 are also associated with autosomal dominant PD. Mutations in the glucocerebrosidase (GBA) gene, which encodes an enzyme involved in glycolipid metabolism, have also been linked to sporadic PD (Maulik et al. 2017). Mutations in UCHLI, the gene encoding ubiquitin carboxyl-terminal hydrolase L1 enzyme, which is responsible for ubiquitin recycling, has also been linked to early-onset familial PD. The numerosity and diversity of these causative genes presents significant challenges to researchers seeking to understand the molecular mechanisms underlying Parkinson's disease pathogenesis.

LRRK2 and Parkinson's Disease

Leucine rich repeat kinase-2 (LRRK2) is a large (280 kDa), multidomain protein with GTPase and kinase domains (West et al. 2006; Yao et al. 2010). The gene encoding LRRK2 is located within the PARK8 locus on chromosome 12 (Azeggagh and Berwick 2021). It is expressed by neurons in the cerebral cortex, as well as the striatum, a region implicated in the pathogenesis of PD (West et al. 2006). It is normally involved in apoptosis, protein translation, MAP kinase pathways, and cytoskeleton maintenance. Mutations in LRRK2 have been identified by genome wide association studies to be the most common genetic cause of PD as well as a cause of sporadic PD (Liu et al. 2011; Yao et al. 2020). It should be noted that LRRK2 PD is symptomatically indistinguishable from other forms of genetic and idiopathic PD (West et al. 2006). LRRK2 PD represents approximately 5% of familial cases worldwide, though this proportion can reach up to 40% in certain populations such as North African Arabs and Ashkenazi Jews (West et al. 2006; Madureira et al. 2020; Usmani et al. 2021). In some regions, such as in Asia, LRRK2 PD is extremely rare. The G2019S LRRK2 mutation is most common,

affecting the protein's kinase domain (Yao et al. 2010). It is believed to add additional phosphorylation sites near phosphorylation residues in the activation loop, thereby upregulating kinase activity and leading to various neurotoxic effects (West et al. 2006; Yao et al. 2010; Liu et al 2011). Furthermore, the G2019S mutation has been linked to reduced lysosomal autophagy system function, thereby impairing α-synuclein clearance (Poewe et al. 2017).

Brains of many patients with LRRK2-PD demonstrate an α-synuclein-Lewy pathology, thus it is suggested that LRRK2 either directly or indirectly influences α-synuclein aggregation (West et al. 2006; Usmani et al. 2021). This is particularly evident in individuals with the G2019S mutation. The mechanism by which dysfunctional LRRK2 mediates changes in α-synuclein is yet to be conclusively identified, though research has suggested that chaperone-mediated autophagy (CMA) is disrupted (Madureira et al. 2020). CMA, which is responsible for α-synuclein clearance, is dependent upon the protein LAMP2A. This lysosomal protein necessary for substrate internalization is believed to be altered by the LRRK2-G2019S mutation, thereby preventing lysosomal degradation of α-synuclein. This unchecked α-synuclein aggregation facilitates Lewy body formation and eventual neurotoxicity.

C. elegans Anatomy & Physiology

Caenorhabditis elegans (*C. elegans*) is microscopic, free-living roundworm that grows to 1-2mm in length (Cooper and Van Raamsdonk 2018). They primarily exist as self-fertilizing hermaphrodites, capable of rapidly populating a plate with identical progeny. One nematode can produce more than 300 offspring (White et al. 1986). Males, but not females, also exist due to chromosomal nondisjunction. However, these only constitute 0.1-0.2% of worms. The *C. elegans* lifecycle is well defined, with embryos passing through 4 larval stages (L1-L4) before reaching adulthood (Corsi et al. 2015) (fig. 3). From the time of hatching, they reach adulthood

in approximately 52 hours, beginning to reproduce shortly thereafter. Their lifespan is 2-3 weeks, with a 2–3-day period of fertility beginning approximately 12 hours after the L4 to adult molt.

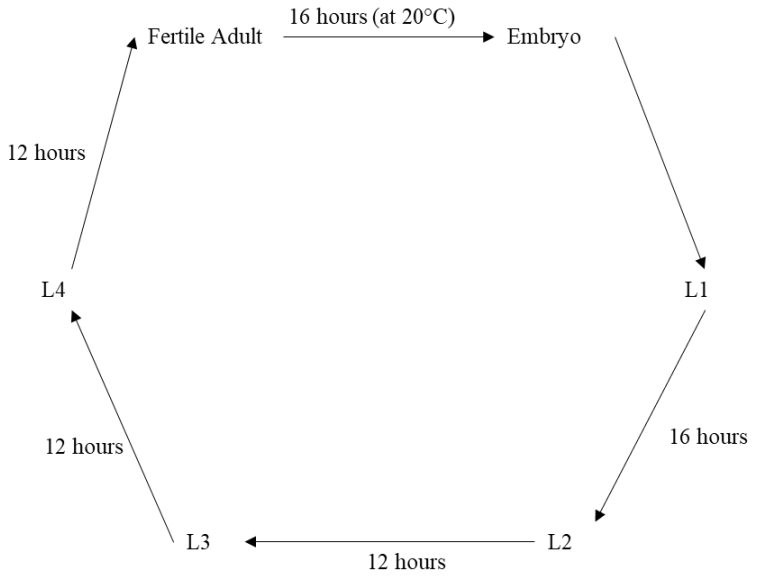

Figure 3. *C. elegans* life cycle

C. elegans' short lifespan of 2-3 weeks enables longitudinal aging studies to be conducted within a relatively short timeframe. They are particularly useful in research due to their small size and relative simplicity (Sawin et al. 2000). There are 959 cells in the entire body, with 302 of them being neurons (Cooper and Van Raamsdonk 2018). Despite their small size, *C. elegans* possess a variety of specialized cell types including muscle cells, excretory cells, and epidermal cells which carry out complex functions (Culetto and Sattelle 2000). The arrangement of these cells is invariant, with all neurons having been mapped via electron micrography, thus making for the most complete connectome of any organism (Cooper and Van Raamsdonk 2018). As such, they are extremely useful in modeling neurological diseases. *C. elegans* are also the first multicellular organism to have their genome completely sequenced. With this it was discovered that 60-80% of human disease-causing genes have nematode orthologs. The

widespread availability of various strains (>20,000 available from the *C. elegans* Genetics Center at the University of Minnesota) further increases their utility. Their transparent cuticle enables visualization of fluorescently labeled proteins, such as neurons expressing green fluorescent protein (GFP) (Cooper and Van Raamsdonk 2018).

C elegans nervous system and dopaminergic behaviors

As aforementioned, the *C. elegans* nervous system is comprised of 302 neurons forming more than 7,000 synapses (Corsi et al. 2015; Cooper and Van Raamsdonk 2018). *C. elegans* neurons are structurally, though not functionally different from mammalian neurons (Corsi et al. 2015). They typically possess only one or two neurites with limited branching. Furthermore, these neurites both send and receive signals, as opposed to the unidirectional communication of human axons and dendrites. Though fewer in number than mammalian nervous systems, glia-like support cells are also present (Corsi et al. 2015). Neurochemically, their function is similar to that of humans and other mammals. *C. elegans* utilize neurotransmitters including acetylcholine, glutamate, γ-amino butyric acid (GABA), serotonin, and of particular interest to Parkinson's research, dopamine. Furthermore, there are conserved receptors, axon guidance molecules, ion channels, and other synaptic elements (Maulik et. al 2017). It is important to note that 8 out of the 302 total neurons are dopaminergic (Cooper and Van Raamsdonk 2018). Neuroendocrine regulation has also been observed, and as such, the *C. elegans* nervous system is commonly used to model human diseases (Corsi et al. 2015). Though anatomically different, their physiological similarities make *C. elegans* a useful tool in biomedical research, particularly in elucidating the molecular mechanisms of disease.

C. elegans engage in complex behaviors including thermotaxis, chemotaxis, mating rituals, social behaviors, and associative learning (Corsi et al. 2015). Some of these are

dopaminergic and are thus mediated by the activity of just 8 neurons. As such, *C. elegans* are an ideal model system in which to correlate neurodegeneration with behavioral changes. Destruction of these neurons, either through gene expression or neurotoxin application, would be expected to produce extinction of such behaviors. Dopaminergic behaviors that have been explored by other members of the Bayne lab in the context of modeling PD include swimming induced paralysis (SWIP), ethanol avoidance, and the basal slowing response (Mody 2021). Swimming induced paralysis is a behavioral pattern in which *C. elegans* become paralyzed after approximately 6 minutes of thrashing in liquid (Cooper and Van Raamsdonk 2018). Impaired dopaminergic function leads to a loss of this response. Ethanol avoidance is a chemotaxis behavior that is also dependent upon intact dopamine signaling. Wildtype worms display negative chemotaxis in response to ethanol, thus avoiding areas of an agar plate seeded with it. Each of these assays are associated with their own imperfections and limitations.

The basal slowing response is also dopamine dependent, as dopamine signaling is necessary for the animal to sense the presence of food. Food deprived *C. elegans* will demonstrate slowing of movement in the presence of a bacterial lawn, while well-fed worms will move the same speed in the absence of bacteria (Sawin et al. 2000). Experimental evidence suggests that a fasting period of just 30 minutes is sufficient to elicit this behavior.

Despite their small size and anatomical differences from human, *C. elegans* remain a useful tool in the investigation of human neurological diseases. Their simple, yet well characterized nervous system, as well as their physiological similarities to humans position them as an excellent candidate for the creation of model systems. Their utility is even more apparent when considering the scale of the human nervous system. The human brain has more than 70 billion neurons, with 10^{10} neurons in the cerebellum alone (White et al. 1986). Each of these

makes thousands of synapses with other neurons. However, this simplicity is also a drawback to the use of *C. elegans*. Their simple body structure and nervous system creates a more simplistic model system than is possible with mammals (Konnova and Swanberg 2018). This leads to eventual limitations in their utility, especially with studies seeking to understand disease mechanisms on a systems level, rather than a cellular or molecular level.

C. elegans as a model system for human diseases

C. elegans are not the only animal used in the modeling of human neurological diseases such as PD. Transgenic rodent models, which can recreate some of the clinical presentations of PD, have also seen widespread use (Konnova and Swanberg 2018). Of the more than 23,000 studies of PD animal models published since 1990, most have used rodents. This is in large part due to their ubiquity within the biomedical research community, as well as the large body of research supporting their use as a PD model system. However, gene editing in rodents is complex, costly, and time consuming. Compounded with the resource intensive nature of rodent care, their use is not always feasible. Non-mammalian (invertebrate) models, such as *Drosophila melanogaster* and *Caenorhabditis elegans* alleviate many of these issues. They have many conserved pathways and mechanisms, making them viable models. Various genes implicated in PD, including PINK1, PARK, DJ-1, and LRRK2 have *C. elegans* homologs as well (Maulik et al. 2017). While α-synuclein is not endogenous to nematodes, expression of the human protein is possible through genetic manipulation. Homologs of mammalian D1 and D2 dopamine receptors are also present. Such biochemical similarities enable the use of *C. elegans* in screening compounds for potential therapeutic utility.

Relative ease in acquiring transgenic *C. elegans*, with more than 20,000 strains commercially available and even more possible through gene editing, also leads to a decreased

need for neurotoxin-based models of Parkinson's disease. Neurotoxic compounds including 6-hydroxydopamine (6-OHDA) and 1-methyl-4-phenyl-1,2,3,6-tetrahydropyridine (MPTP) have historically been used to selectively destroy dopaminergic neurons, thereby generating a Parkinson's-like phenotype (Konnova and Swanberg 2018). While these model systems do have utility, especially in examining toxic exposure as a risk factor for PD, they do not provide the same insights into the molecular mechanisms of disease development afforded by genetic models. Furthermore, the use of transgenic *C. elegans* is superior to neurotoxins from an environmental health and safety perspective.

The utility of *C. elegans* as a tool for investigating LRRK2 induced PD was demonstrated by Yao et al. in their 2010 study of several strains. These included the wildtype N2 and dopamine deficient cat-2 and LRRK2 mutants. The cat-2 gene encodes tyrosine-3-monooxygenase, a rate limiting enzyme for dopamine synthesis that catalyzes the conversion of tyrosine into L-DOPA, the biosynthetic precursor to dopamine (Sawin et al. 2000; Yao et al. 2010; Omura et al. 2012). These worm strains have reduced cat-2 expression, thereby limiting dopamine production. The presence (or diminishing) of the basal slowing response was used as a metric of DA neuron degeneration secondary to the neurotoxic effects of LRRK2 (Yao et al. 2010). As expected, wildtype N2 worms demonstrated an intact basal slowing response, while dopamine deficient cat-2 mutants demonstrated a loss of the behavior. These controls indicate that dopamine deficiency does cause observable deficits in the basal slowing response. With these findings, the researchers moved on to testing LRRK2 mutants, which all showed neuronal loss beginning on day 2 and worsening from days 5-9. With this they observed a progressive loss of the basal slowing response, suggesting that the degree of neurodegeneration is proportional to the degree of behavioral deficit. LRRK2 G2019S worms showed an approximately 50%

reduction in DA, while cat-2 worms showed an approximately 75% reduction in DA compared to N2 worms. The role of LRRK2 kinase overactivity in mediating neurodegeneration was further demonstrated in a study by Liu and colleagues, wherein researchers knocked down its activity via the induction of a loss of function mutation (Liu et al. 2011). The D19941 mutation in LRRK2 leads to mutation of an aspartic acid residue, which inhibits kinase function. This resulted in a reduction in neurodegeneration compared to G2019S mutant worms, as determined via fluorescent microscopy of DA neurons. These findings support the notion that LRRK2 kinase domain overactivity, which can be mediated by the G2019S mutation, is a potential cause of PD.

LRRK2 as a therapeutic Target

The primary treatment for Parkinson's disease is pharmacological dopamine supplementation with levodopa (L-Dopa), a dopamine precursor molecule (Girault and Greengard 2004; Poewe et al. 2017). Introduced in the 1960s, this drug compensates for the loss of dopamine producing neurons and can help alleviate symptoms. However, it does not interrupt the underlying disease processes. Thus, patients receiving L-Dopa therapy will still experience a gradual increase in disability. As our knowledge of the mechanisms underlying PD grows, new possibilities for treatments have emerged. Currently, clinical trials are underway examining the effectiveness of the drug Ambroxol, as well as gene therapy, to improve delivery of the lysosomal enzyme glucosylceramidase (Azeggagh and Berwick 2021). This is believed to improve α-synuclein clearance via restoration of lysosomal autophagy system functionality. Another compound, Anle138b, is being investigated for its ability to inhibit α-synuclein aggregation.

A substantial body of research has linked increased activity of the kinase domain of LRRK2 with the pathogenesis of Parkinson's disease (Yao et al. 2010; Liu et al. 2011;

Madureira et al. 2020). With this has come the identification of LRRK2 as a potential therapeutic target. Since upregulation of kinase activity is believed to be the mechanism through which LRRK2 mutations exert neurotoxic effects, it stands to reason that kinase inhibitors may have therapeutic benefit. Several compounds have been identified, including LRRK2-IN1, TTT-3002, H-153, and Sorafenib. One study conducted using human cell lines, assessed the effectiveness of TTT-3002 as an inhibitor of LRRK2 kinase activity (Yao et al. 2012). The researchers found that TTT-3002 is a potent, effective kinase inhibitor, thus posing it as a candidate for further evaluation. As part of the same study, the researchers moved on to testing the efficacy of LRRK2-IN1, H-153, and TTT-3002 In transgenic *C. elegans* expressing the G2019S mutation. It was found that, with treatment between the L1-L4 stages, TTT-3002 and LRRK2-IN1 demonstrated a dose-response relationship with restoration of the basal slowing response. Even when administered between adult day 2-3, once deterioration of the basal slowing response had already manifested, TTT-3002 was able to rescue dopaminergic behaviors. When examined under fluorescent microscopy, DA neurons treated with TTT-3002 demonstrated up to 80% survival on adult day 9, which was a significant increase over the 40% survival in the control group. Perhaps the most compelling finding from this study is the implication that treatment with kinase inhibitors has therapeutic benefits both before and after onset of symptoms. The neuroprotective effects exerted by these kinase inhibitors may be able to arrest some of the processes ultimately leading to the death of DA neurons in the substantia nigra, thereby interrupting disease progression.

Shortly after the identification of LRRK2 kinase overactivity as a contributor to PD pathogenesis, pharmaceutical researchers began investigating potential LRRK2 targeting drugs (Azeggagh and Berwick 2021). Such work has been in progress for upwards of 10 years and has

yielded several potential therapeutic compounds. A majority of these have been class 1 kinase inhibitors, which compete with ATP for its binding pocket in the kinase domain. Two such drugs have progressed to phase 1 clinical trials: DNL-201 and DNL-151 from Denali Therapeutics. In phase 1a trials, both were well tolerated by healthy subjects and found to exhibit effects on LRRk2 activity and lysosomal function. Phase 1b trials involving patients with PD have yielded similarly promising results. As such, Denali is moving forward with the expansion of clinical trials. Other pharmaceutical companies, including Cerevel and Merck, also have LRRK2 kinase inhibitors in the early stages of development, though their continued development is likely dependent upon the results of Denali's studies.

Research Goals

The goal of this research is to develop a model system of LRRK2 Parkinson's disease using *C. elegans*. By developing a robust behavioral assay capable of quantifying the degree of motor deficits, as well as correlating these observations with neuronal morphology, we can assess the therapeutic potential of various kinase inhibitors.

Why Basal Slowing

Prior work by members of the Bayne lab has centered around exploring options for assays assessing dopaminergic behaviors in *C. elegans.* The ethanol avoidance, swimming-induced paralysis (SWIP) and movement-over-alternate-terrain (MOAT) assays were found to be unsuitable for modeling the progressive motor deficits associated with PD (Mody 2021). Wildtype and LRRK2 mutant worms did not demonstrate phenotypic differences in an ethanol avoidance assay. Because of a natural reduction in the swimming-induced-paralysis (SWIP) behavior over time, this assay would not be viable for conducting longitudinal studies. Finally, the MOAT assay did not yield data useful for determining dopaminergic function. Based on

work by Yao and colleagues (2010 and 2012), the use of the basal slowing response as a metric of dopaminergic neurodegeneration was selected for further investigation. Furthermore, This assay is ideal due to its accessibility, simplicity, and ability to be expanded to a large scale. Using open-source software and readily available components, researchers the Illinois State University developed a worm tracking system for only $40 (Leonard and Vidal-Gadea 2021). A variation of this apparatus was constructed and utilized in the completion of this research. This system is also relatively easy to use, automating several aspects of data acquisition and processing. Because of this high degree of automation, it is possible to scale this behavioral assay to assess larger worm populations with minimal changes to the researcher's workflow. Such attributes give the basal slowing assay potential as a tool for drug screening, particularly in laboratories with limited resources.

Fluorescent Microscopy

JVR168 *C. elegans* express green fluorescent protein in their dopaminergic neurons, as well as the human G2019S LRRK2 mutation (Maulik et al. 2017). Thus, it is possible to visualize the degeneration of these neurons over time. Axonal degradation due to Parkinson's disease follows a predictable pattern, which begins with dystrophy, or swelling along the length of the neurite (Kneysberg et al. 2016). Spheroids, or localized widening of the axon separated by areas of thinning, are created in the process of segmentation. Over time, these thin areas are severed, thereby leading to axonal punctation. Such a process continues until the remaining particles are degraded beyond the point of detection. To yield statistically valid results, it is necessary to empirically, rather than qualitatively, describe this degeneration. In their 2016 paper, Kneysberg and colleagues reported on the utility of ImageJ in quantitative image analysis of neurons in both brain sections and primary culture from a 6-OHDA rat model of PD. Because

of the predictable pattern of neurodegeneration in this model system, they proposed the following as metrics of neuronal change: the number of particles composing the image (particle count), the average size of these particles, and the total area of the particles. Changes in the number and size of individual particles composing an axon or soma indicate dystrophy, spheroid formation, and segmentation. Measuring the total area of all particles, which indicates the total area of the axon or soma, is used to assess for overall degradation of the cell. It was experimentally verified that 6-OHDA lesioning of the neostriatum was associated with a significant decrease in average particle size and total neuron area, as well as a significant increase in total particle count. This is consistent with the predicted pattern of neurodegeneration, wherein the axon becomes punctuated and degrades into many smaller particles. This study aims to verify these results, as well as assess the relationship between neuronal morphology and changes in dopaminergic behaviors.

Materials & Methods

Worm Husbandry

Stocks of several *C. elegans* strains, obtained from the *Caenorhabditis* Genetics Center at the University of Minnesota, were maintained, and assayed in the conduct of this research (Table 1).

Table 1: *C. elegans* strains employed in this research

Strain	Genotype & Phenotype
N2	Wildtype (no deficits in dopaminergic functions)
MT15620	n4547 mutation in cat-2, resulting in a 1,010 bp deletion in gene encoding tyrosine-3-monooxygenase. Dopamine deficient
JVR105	Pdat-1::GFP, Intact dopaminergic behaviors
JVR168	Pdat-1::GFP, Pdat-1::LRRK2::G2019S Time dependent degradation of dopaminergic neurons secondary to LRRK2 overexpression

Worms were maintained on Nematode Growth Media (NGM) agar seeded with a lawn of *E. coli* OP50 bacteria at 15°C. New plates were prepared via "chunking," wherein a flame-sterilized spatula is used to transfer a small piece of agar, populated with worms, onto a fresh NGM plate. The transfer of individual worms was accomplished via picking with a flame-sterilized platinum wire.

Age synchronicity, necessary for behavioral assays, was achieved via spot bleaching or batch bleaching. To generate an age synchronized stock of L1s, the process of batch bleaching was utilized. Gravid adults were washed from an NGM plate and treated with 20% alkaline hypochlorite solution, yielding eggs, which hatch into L1s overnight with agitation. These were then transferred to a fresh NGM plate where they would continue development into adults or stored at 10°C until needed. A smaller scale procedure, spot bleaching, was utilized to remove contamination from a stock plate. Herein individual gravid worms were picked into a small drop

of alkaline hypochlorite solution placed on the edge of a new NGM plate. When necessary to maintain age synchronization of a population, worms were maintained on OP50 seeded NGM with 0.02 mg/mL 5-Fluorodeoxyuridine (Yao et al. 2010). This DNA synthesis inhibitor suppresses progeny growth by preventing the hatching of eggs.

Genotyping

To ensure that stocks were not mixed or mislabeled, N2 and MT worms were genotyped via PCR and gel electrophoresis. 3 worms of each strain were added to a PCR tube containing deionized H_2O and worm lysis buffer (InVivo Biosystems) and incubated for 10 minutes at 75°C and 95°C. This yielded template DNA which was then amplified via PCR at an annealing temperature of 64.8°C. Forward (5' – AGTTTTCGGATCCCCGAAGG - 3') and reverse (5' - AGAGATCACGGATCACAAGAGCA - 3') primers, designed to amplify the entirety of cat-2, were selected using NCBI PrimerBLAST. A sample of PCR product from each strain was run on a 1% agarose gel at 80V, 2A, for 120 minutes to ascertain the presence of a deletion in the cat-2 gene. Another sample of PCR product from each strain was set aside for sequencing. DNA was purified using the New England Biolabs Monarch PCR & DNA cleanup kit protocol. The Applied Biosystems BigDye Terminator V3.1 cycle sequencing kit was then utilized, followed by an ethanol precipitation, and loading into sequencer with the same PCR primers.

Basal Slowing Assay

This basal slowing assay technique was adapted from Yao et al. 2010. Approximately 6 age synchronized worms were picked into the lid of a microcentrifuge tube containing 40 µL M9 buffer. Worms were spun down and subsequently washed twice with M9 buffer to remove any bacteria. These worms were then incubated at room temperature for a 30-minute fasting period. Using a glass pipet, worms were transferred onto a 6cm NGM plate. A total of 4 plates were

utilized in each assay, 2 seeded with OP50, and 2 unseeded. A rectangle of filter paper with an 8mm x 6mm window was placed around the worms. 100 mM $CuSO_4$ was then applied dropwise to the filter paper, forming a barrier to prevent worms from leaving the microscope field. If excess buffer was present within the window, it was soaked up using the corner of a kimwipe. Using an MTWOTHAN USB microscope and iSpy® video capture software, videos of worm movements were captured in 30 second intervals, for a total of 2 minutes of footage per strain.

Videos were then imported into the image processing program ImageJ. To facilitate video analysis, brightness and contrast were adjusted to reduce the visibility of tracks in the agar, followed by removal of background noise via the background subtraction tool. After conversion of the footage into black and white binary using the threshold function, the plugin WrmTrck was run to analyze worm movement, with data collected on maximum and average velocity, track length, and body lengths traveled per second. Data were aggregated in Microsoft Excel and imported into R for statistical analysis and visualization. Data were grouped by worm strain, age, and plate seeding condition. Mean values for these 3 locomotor parameters were calculated, as were the basal slowing ratios for each strain using the following formula:

(Average speed in absence of bacteria – Average speed in presence of bacteria) / Average speed in presence of bacteria. Unpaired samples t-tests, as well as Welch's t-tests, ANOVAs, and Wilcox tests where appropriate, were employed to compare the mean average speeds, mean maximum speeds, and mean body lengths per second (BLPS) across tracks on seeded and unseeded plates for wildtype N2 worms. Based on these results, average speed was selected as the ideal metric for assessment of the basal slowing response.

Fluorescent Microscopy

Worms were picked into a 2 µL drop of Levamisole on a chilled glass slide and surrounded with InVivo Biosystems NemaGel. A coverslip was applied, and the slide was incubated at 25°C until solidified. A Zeiss Axiovert microscope fitted with camera and AxioVision software was utilized for fluorescent microscopy of JVR105 and JVR168 cephalic dopaminergic neurons. Images were captured using a 1.3 second exposure under 20X magnification with HE GFP illumination. A total of 5 worms per strain per time point were imaged and analyzed. The image processing software ImageJ was utilized to analyze neuronal morphology. The "Analyze Particles" function of ImageJ was utilized to collect data on manually selected areas of each image. The following metrics of neuronal degeneration were captured for both the whole neuron (soma + axon) and the axon alone: total number of particles, average particle size, and total area. These data were averaged and compared across ages and worm strains.

Results

N2 & MT Genotyping

Gel electrophoresis of N2 and cat-2 PCR products yielded an expected pattern of banding, wherein an approximately 1 kb deletion was noted in the cat-2 lane. Sequencing of the cat-2 gene of MT15620 worms reflected a 1,010 base pair deletion in comparison to wildtype N2 worms. This verified the identity of the N2 and MT15620 worms utilized in this experiment, ensuring their validity as positive and negative controls.

A

B

agttttcggatccccgaaggatctttttccaaaatttatag**actgggagcattcaggctagagtttataggtttcccattgaaacaaactccagagcttgacctttgattcttgtccaatgtccttttacttccgtccgtcttgagaatctgatcttcatatccaaaattgactggtaatcaacaacaagcggccgacaaaaattgggctagcgttggcgatcgtgaaagcgtcgaatttcatcttgttaataagaagttttcctgacattgtataaatcaatttatgctcaaaaagaaaatccgatttaaatgtctcaaaaaatagacatttaaaaaaactataataaaacaacttgacaaaagtcaaatttttggaataggaaccatagaagatctccaataacccggaaattttatttaaaaactatgtgaagtcacacctgtct-**

*tcatttctccttttgttaattcagtataaaatcgtcccacgtcatatctacagtaccccgtgcttttcaaaaagtgcatttcacctgaacaactccttccatggaatcaatgctatattacacaataacaatgcacattcatatgctccaaagtatgcaatgatgatttgatacggaaggaaatgtggtgtctctctttcagagtactccataacacagcaacaggagcaacaattatctcttctcactgtcgttgttggcgtggggacccctgaaaaattggaagaggaa*ATGTTTTTGCGGTATATGCGGAGGCGGGGCTCTGGAGAGGATCAC*gtaaattctgttcaaatatatttcaggtattcgttaggctttcgttcgttttctagttcaacgtggtctccctggtaactaaaaattaaaaacttgaaaaatagaatttccgtgatttttctgatatttgacctcgaaaacaatgttctttgtgttgtattctcagacaacctcatcaacacacacttttataatatctatagtaaaaaagaatagtatgagaagtcgaacagttaatgtgttattcaagtggaatgtgtgtatatatattctaggaagttttcatgaaaattttcaaattttagtgttttctttgagttttggcacattataacgcattaccaactaatttttcatacgctaacattctaaataatgtttgaaagtacctctacaaaacgtacatactaactaaattgagtcacgtaacactgcaattactattgatttactaaaacaatcactgtgttcactttcatatgctgggttatcagttctcggccaataactttctcaataccgtctaaccatctacagtaacccttcagaagtgtcgtctccattgtcaaaactaattgcggcggtgaacgtcgcaaggaacgtctcaattaacatgtcgtcactaaccaacaatactttcatggtaacttagaattaacaccctaagtg-*

atcattttgaaaatccgacctttttgcgaattaaaaaaaaagaaaacgaaaatcgaaatagaagccattaaagttcaaaaacatagaaaagttgagtttttcaatttctaggaggaagaacctcgcggtgtcacagtcatcgccaccaaagtagccgagaactccaaaaatccacgtcgctacagtttggtgcaccaagcgagttgtgagactcaacatcataagggtatacggagacagaacacaattcaacaccgaaaacagctcaccgatcagatgaggtgtcagaaggtacagtaatccatacaagctct**tgtgatccgtgatctct

Primer Sequences

MT PCR product sequence

Deletion (Includes exon 1)

Figure 4. MT15620 C. elegans possess a 1,010 bp deletion in cat-2. A. Sequencing of MT15620 worms revealed a 1,010 bp deletion **B.** This deletion was found to begin prior to exon 1 and terminate prior to allele n4547 on exon 2 of the cat-2 gene. This results in a loss of tyrosine-3-monooxygenase expression and subsequent dopaminergic behaviors.

Adapted from WormBase.

N2 L4 Basal Slowing Assay

Mean values for body lengths per second, average speed, and maximum speed for seeded and unseeded conditions were calculated in R and reported in table 2 and figure 5.

Table 2. N2 L4 tracking parameters

Parameter	Plate	Mean
Body Lengths Per Second (BLPS)	Unseeded	0.171
	Seeded	0.0746
Average Speed (mm/sec)	Unseeded	0.223
	Seeded	0.0844
Maximum Speed (mm/sec)	Unseeded	0.423
	Seeded	0.337

An F-test was performed for each of these metrics to assess for homoscedasticity. Because of the unequal variances between the seeded and unseeded conditions of both average speed and body lengths per second (BLPS), a Welch's t-test was utilized to determine if a statistically significant difference existed across the seeded and unseeded conditions. A significant decrease in average speed was noted from the unseeded plate to the seeded plate ($p=0.0045$). A significant decrease in body lengths per second was also noted ($p=0.0037$). Assuming equal variances based on the results of an F-test, an unpaired samples t-test was utilized to assess maximum speed. No significant difference was observed in the maximum speed of worms on seeded and unseeded plates ($p=0.25$).

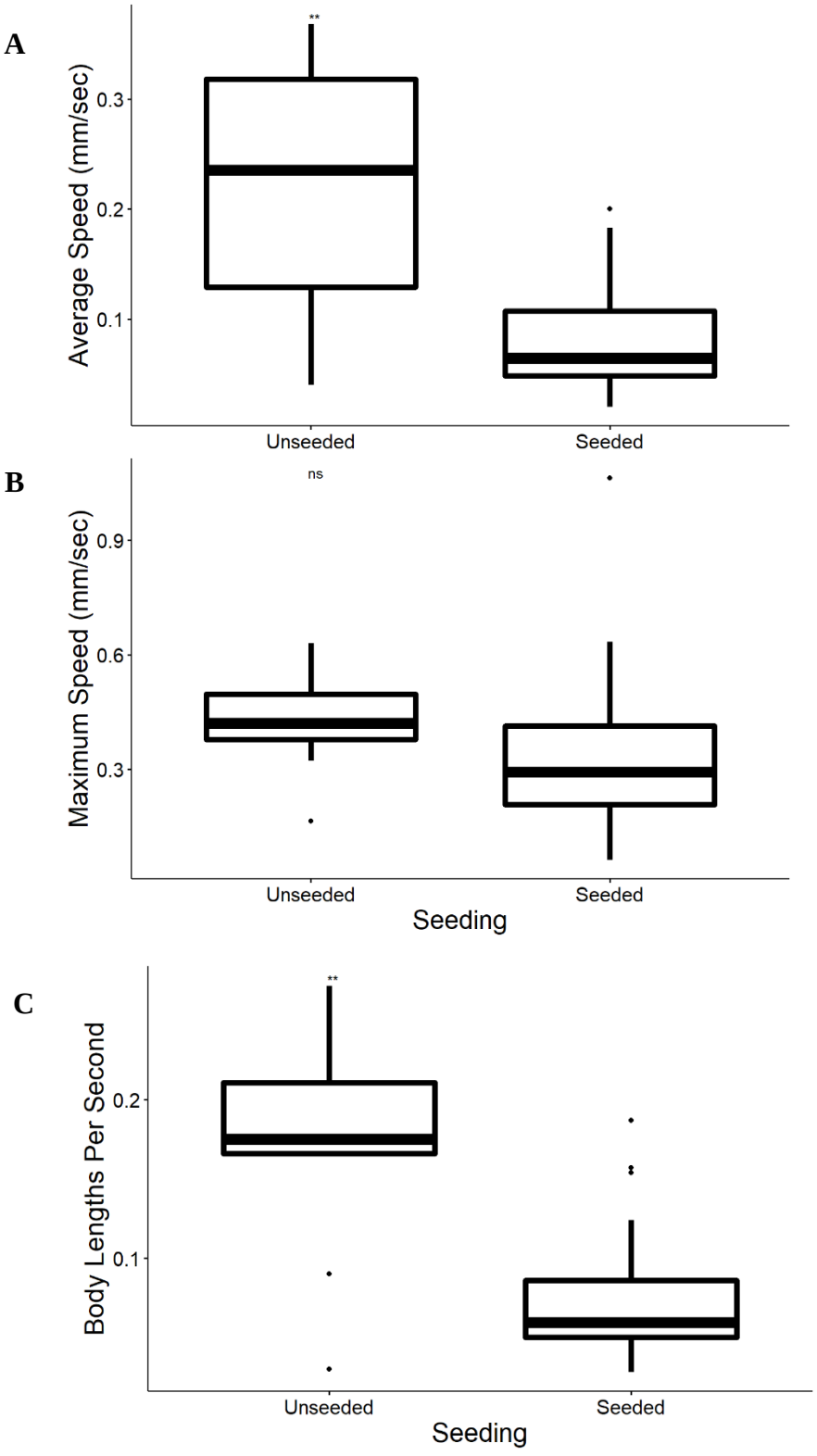

Figure 5. N2 L4 tracking parameters. (A) Mean average speed, (B) body lengths per second, and (C) maximum speed of N2 *C. elegans* reported on unseeded vs. seeded plates. ** Indicates statistical significance ($p<0.05$). Significant decreases in average speed and body lengths per second from unseeded to seeded plates were observed.

MT15620 Basal slowing assay

A series of basal slowing assays was carried out on an age synchronized stock of MT15620 worms at the L4, A4, and A7 life stages. Mean values of body lengths per second, average speed, and maximum speed are reported in table and figure 5.

Table 3 Average Speed (mm/sec)

Life Stage	Unseeded	Seeded
L4	0.0835	0.0761
A4	0.149	0.0890
A7	0.0706	0.0997

Table 4 Body Lengths Per Second (BLPS)

Life Stage	Unseeded	Seeded
L4	0.0876	0.0682
A4	0.105	0.0816
A7	0.0593	0.0691

Table 5 Maximum Speed (mm/sec)

Life Stage	Unseeded	Seeded
L4	0.258	0.274
A4	0.486	0.381
A7	0.324	0.417

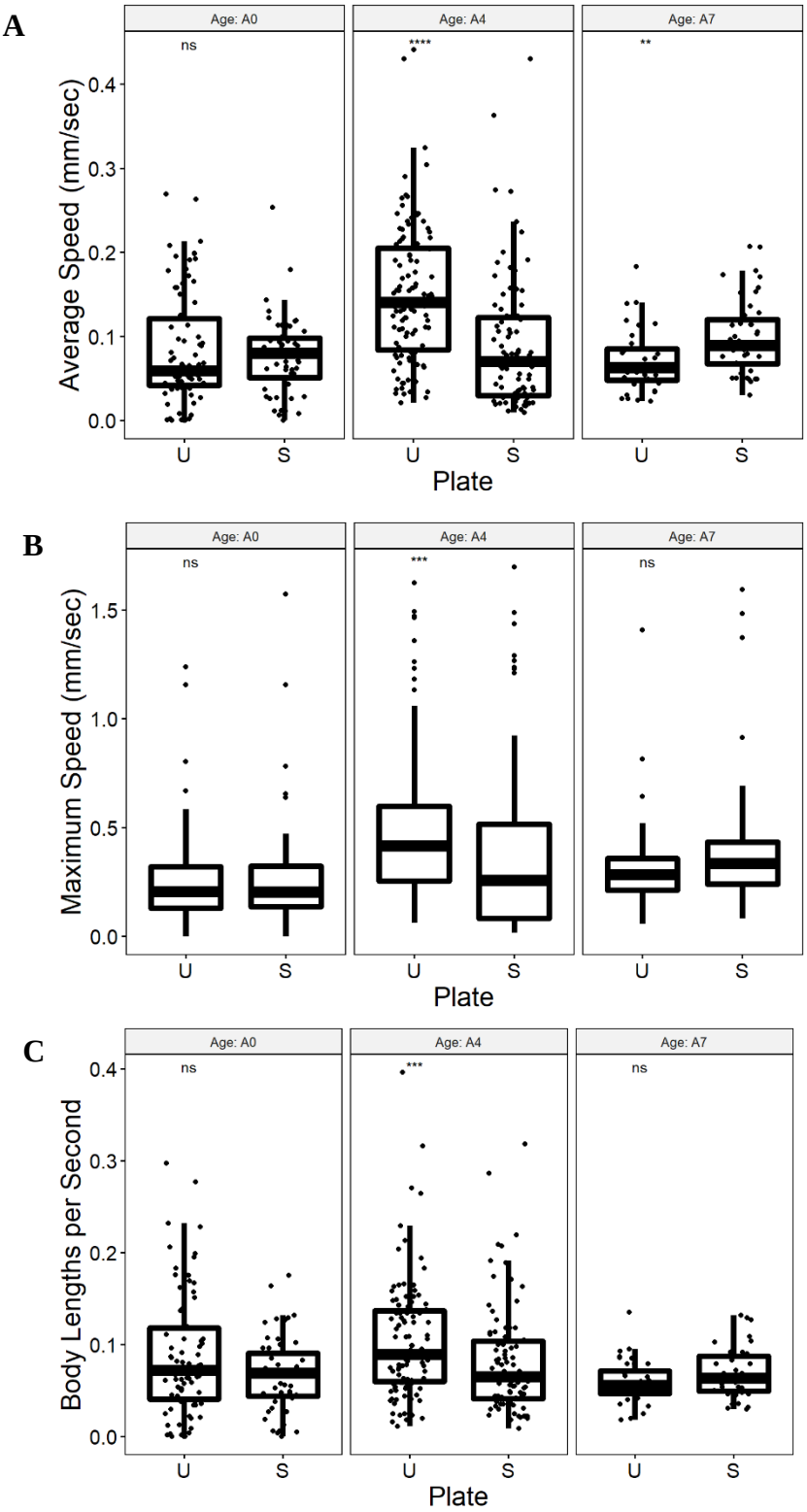

Figure 6. MT15620 tracking parameters. Statistical significance ($p<0.05$) indicated by **. U=Unseeded, S=Seeded (A) Significant differences in average speed observed on adult days 4 and 7. (B) Significant differences in maximum speed observed on adult day 4. (C) Significant differences in body lengths per second (BLPS) observed on adult day 4.

A Wilcox signed rank test was employed to evaluate the statistical significance ($p<0.05$) of differences between seeded and unseeded plate conditions at various life stages. The only statistically significant difference in body lengths per second was observed in adult day 4 worms, wherein worms on the seeded plate exhibited a greater number of body bends per second than those on an unseeded plate ($p=0.0026$). For average speed, significant differences were noted between unseeded and seeded plates at adult day 4 ($p<0.001$) and adult day 7 ($p=0.0054$). A significant decrease in average speed between unseeded and unseeded was noted on day 4, while a significant increase was noted on day 7. A significant difference in maximum speed was only noted for adult day 4 worms ($p<0.001$).

JVR105 Basal Slowing Assay

A series of basal slowing assays was carried out on an age synchronized stock of JVR015 A4 and A7 life stages. Videos of JVR105 worms at the L4 stage were excluded from analysis, as the small size and transparency of the worms did not provide enough contrast to be visible under the USB microscope. Average speed and body lengths per second data for JVR105 worms are reported in table and figure 6. Based on the results of the N2 and MT15620 assays, maximum speed was omitted as a variable due to its lack of significance.

A Wilcox signed rank test was utilized to evaluate the statistical significance ($p<0.05$) of differences between seeded and unseeded plate conditions at various life stages. On adult day 3, no statistically significant differences were observed in average speed or body lengths per second ($p= 0.319$ and 0.312 respectively). On adult day 7, a statistically significant increase in both body lengths per second observed ($p=0.000128$) and average speed ($p=0.000262$) between unseeded and seeded plates was observed.

Table 6. JVR105 Tracking Parameters

Life Stage	Parameter	Plate	Mean
A3	Body Lengths Per Second (BLPS)	Unseeded	0.0990
		Seeded	0.0858
	Average Speed (mm/sec)	Unseeded	0.0862
		Seeded	0.0805
A7	Body Lengths Per Second (BLPS)	Unseeded	0.0513
		Seeded	0.0934
	Average Speed (mm/sec)	Unseeded	0.0629
		Seeded	0.104

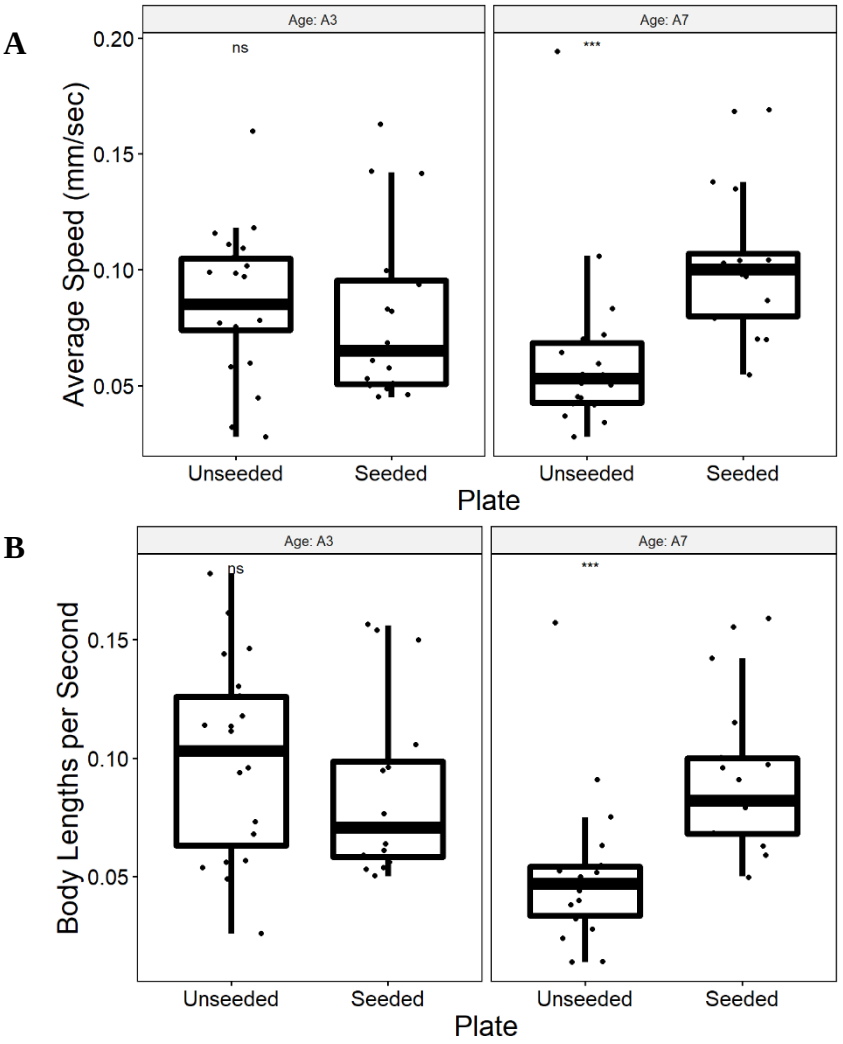

Figure 7. JVR105 tracking parameters. Statistical significance ($p<0.05$) indicated by ** (A) Significant difference in average speed observed on adult day 3. (B) Significant difference in BLPS observed on adult day 4.

JVR168 Basal Slowing Assay

A series of basal slowing assays was carried out on an age synchronized stock of JVR015 A4 and A7 life stages. Average speed and body lengths per second data for JVR168 worms are reported in table and figure 7. A Wilcox signed rank test was employed to evaluate the statistical significance ($p<0.05$) of differences between seeded and unseeded plate conditions at various life stages. Statistically significant differences in average speed were noted in worms at larval stage 4 ($p=0.0317$) and adult day 7 ($p=0.00503$), with worms exhibiting a greater average speed of movement on seeded plates compared to unseeded. A significant increase in body lengths per second on seeded compared to unseeded plates was noted on adult day 7 ($p=0.00273$). Otherwise, no significant differences were noted between seeded and unseeded plates.

Table 7. JVR168 Tracking Parameters

Life Stage	Parameter	Plate	Mean
L4	Body Lengths Per Second (BLPS)	Unseeded	0.108
		Seeded	0.165
	Average Speed (mm/sec)	Unseeded	0.0993
		Seeded	0.148
A3	Body Lengths Per Second (BLPS)	Unseeded	0.058
		Seeded	0.066
	Average Speed (mm/sec)	Unseeded	0.084
		Seeded	0.096
A7	Body Lengths Per Second (BLPS)	Unseeded	0.020
		Seeded	0.0393
	Average Speed (mm/sec)	Unseeded	0.029
		Seeded	0.051

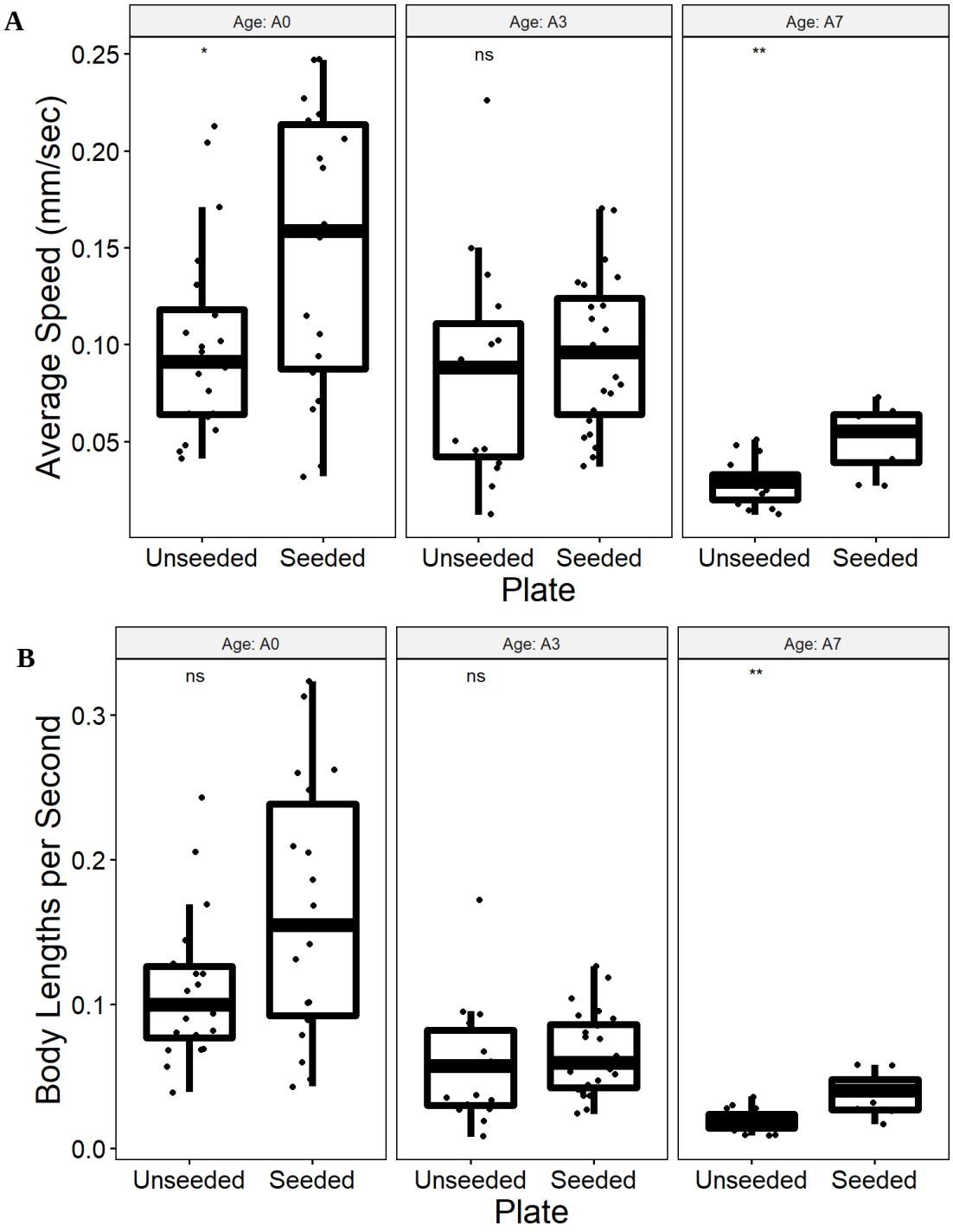

Figure 8. JVR168 tracking parameters. Statistical significance ($p<0.05$) indicated by ** (A) Significant difference in average speed observed at larval stage 4 adult day 7. (B) Significant difference in BLPS observed on adult day 7.

Fluorescent microscopy and DA neuron morphology analysis

To assess time dependent neurodegeneration, the cephalic dopaminergic neurons of JVR105 and JVR168 worms were imaged under 20X magnification and GFP illumination. These images are presented in figures 9 and 10 respectively. Mean total area, particle count, and average particle size of neurons and axons for both strains are reported in table 9.

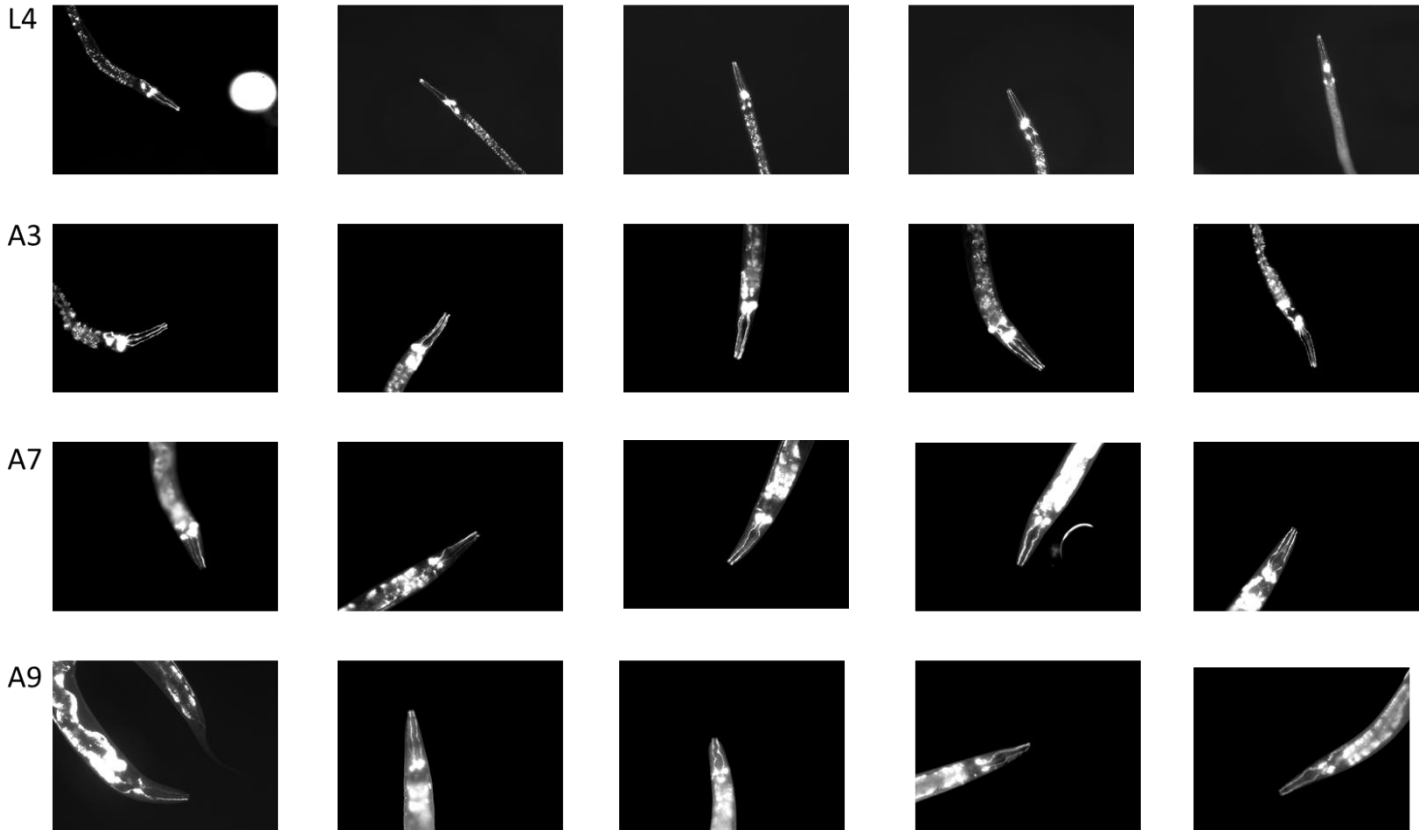

Figure 9. Fluorescent microscopy of JVR105 dopaminergic neurons

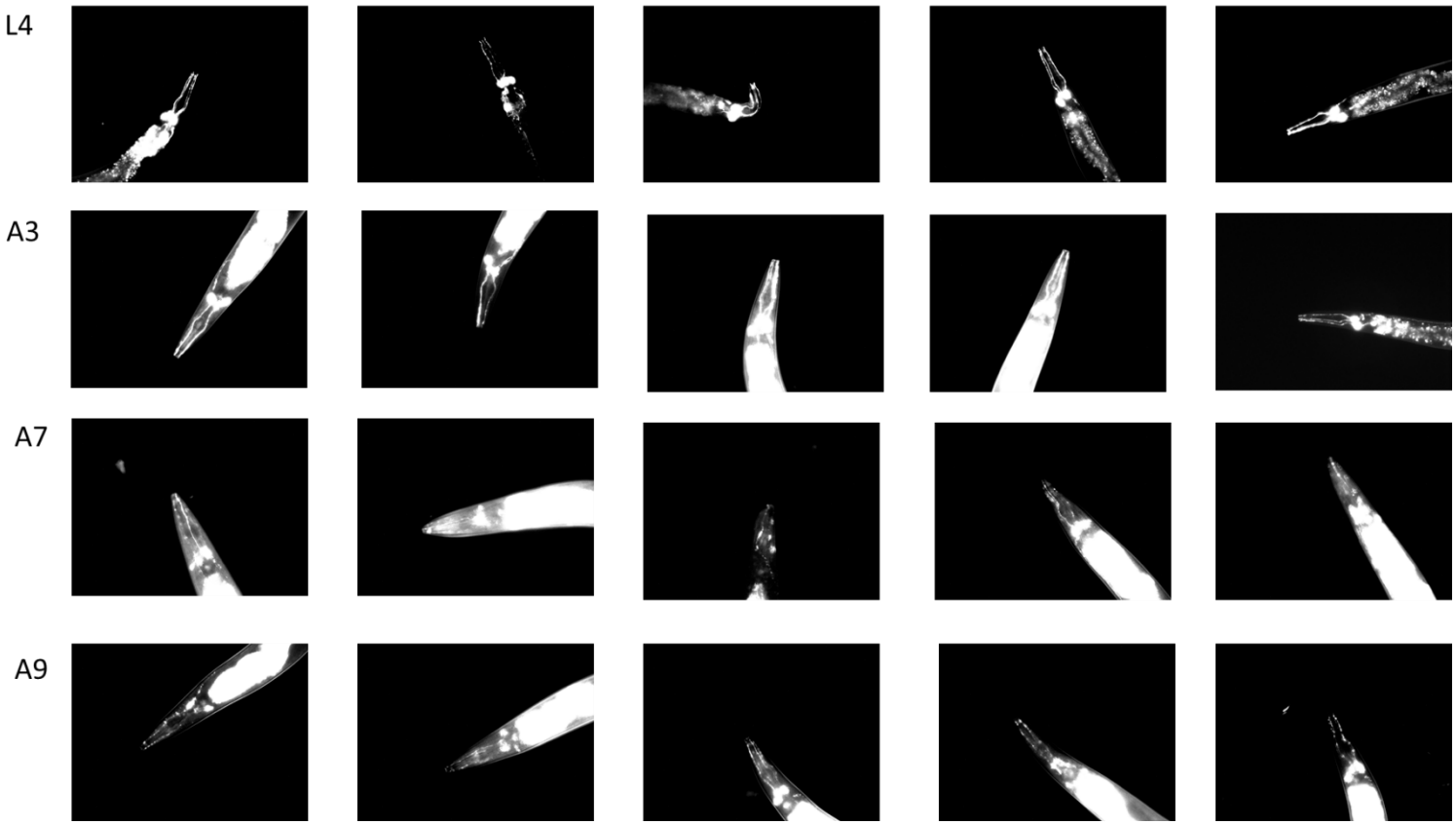

Figure 10. Fluorescent microscopy of JVR168 dopaminergic neurons

Table 8. Fluorescent Microscopy Data

Strain	Age	Particle Count (Axon)	Particle Count (Axon + Soma)	Total Area (Axon)	Total Area (Axon + Soma)	Average Particle Size (Axon)	Average Particle Size (Axon + Soma)
JVR168	L4	35.8	48.8	5242.4	13133	205.8	300.7
	A3	72.4	152	7439.2	30533	112.5	226.8
	A7	189	208	3544.8	13164	19.70	64.13
	A9	139	229	2580.2	10929	19.06	51.38
JVR105	L4	24	27	1773.6	5809	80.41	580.9
	A3	24.6	36.6	6552.4	14342.2	283.843	427.3
	A7	38.8	53.2	4870.2	13942.6	147.5324	285.2
	A9	26.2	43.8	3475	11497	164.6934	311.6

Qualitatively examining the images, minimal change is noted in axonal morphology across the JVR105 lifespan. No increase in dystrophy, spheroid formation, or dystrophy was noted from larval stage 4 through adult day 9. Figure 11 shows trendlines of these 3 variables in JVR105 worms, which do not carry any PD mutations. Despite an apparent increase in the number of particles composing both the axon and entire neuron, no significant differences were observed between life stages as verified by a one-way ANOVA ($p=0.108$ and 0.11 respectively). A significant increase in axonal particle size was observed between the L4 and A3 life stages ($p=0.027$), though no other significant differences were observed. Significant increases in total area of both the axon and axon + soma ($p<0.001$ for both) were observed between larval stage 4

and adult day 3. This was followed by a downward trend, evident in both the axon and soma. A significant decrease in total axon area was noted between adult day 3 and adult day 9 (p=0.008), though this decline was no longer statistically significant for the axon + soma calculations.

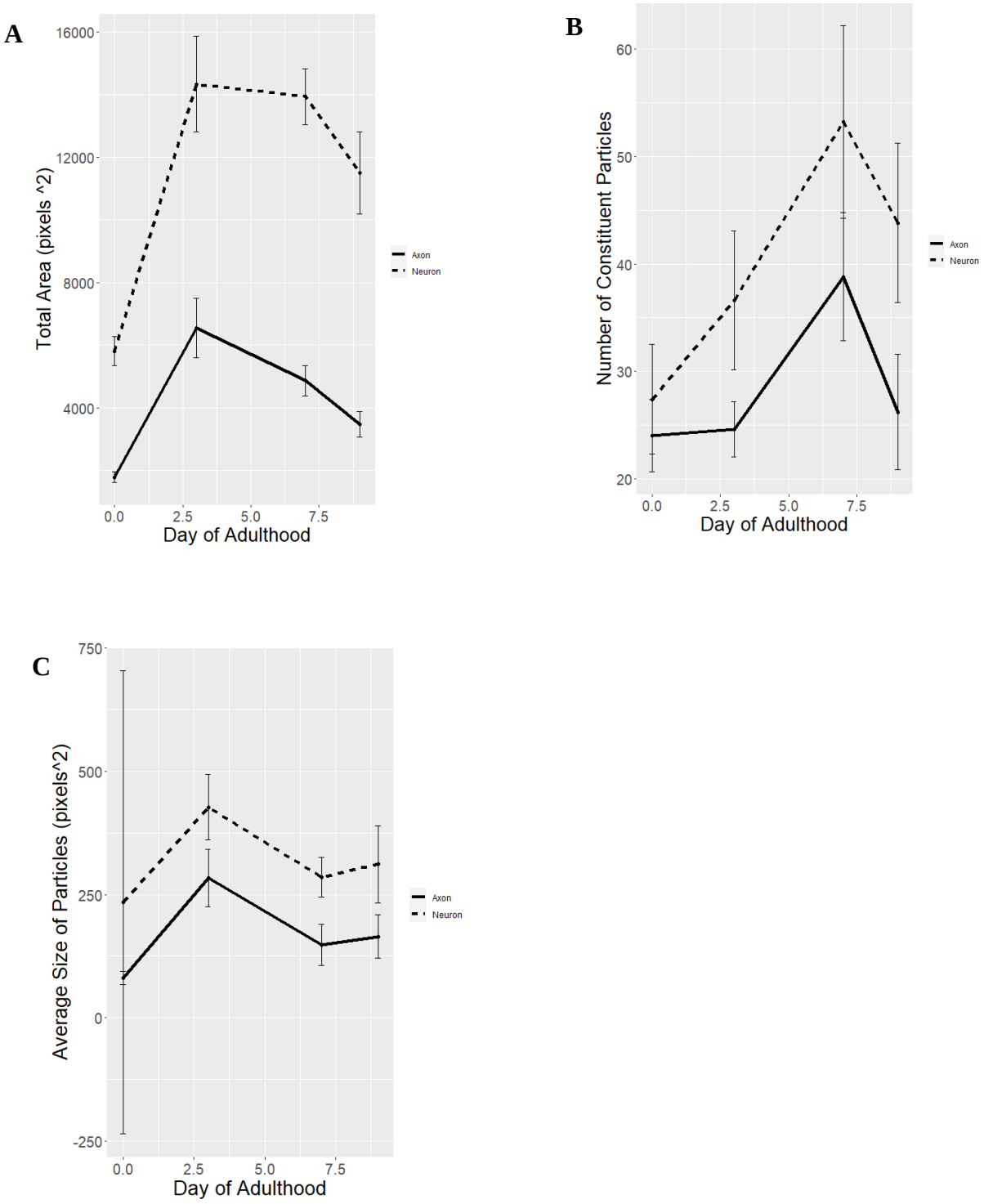

Figure 11. JVR105 neurodegeneration metrics (A) Number of constituent particles (B) Average size of particles (C) Total area

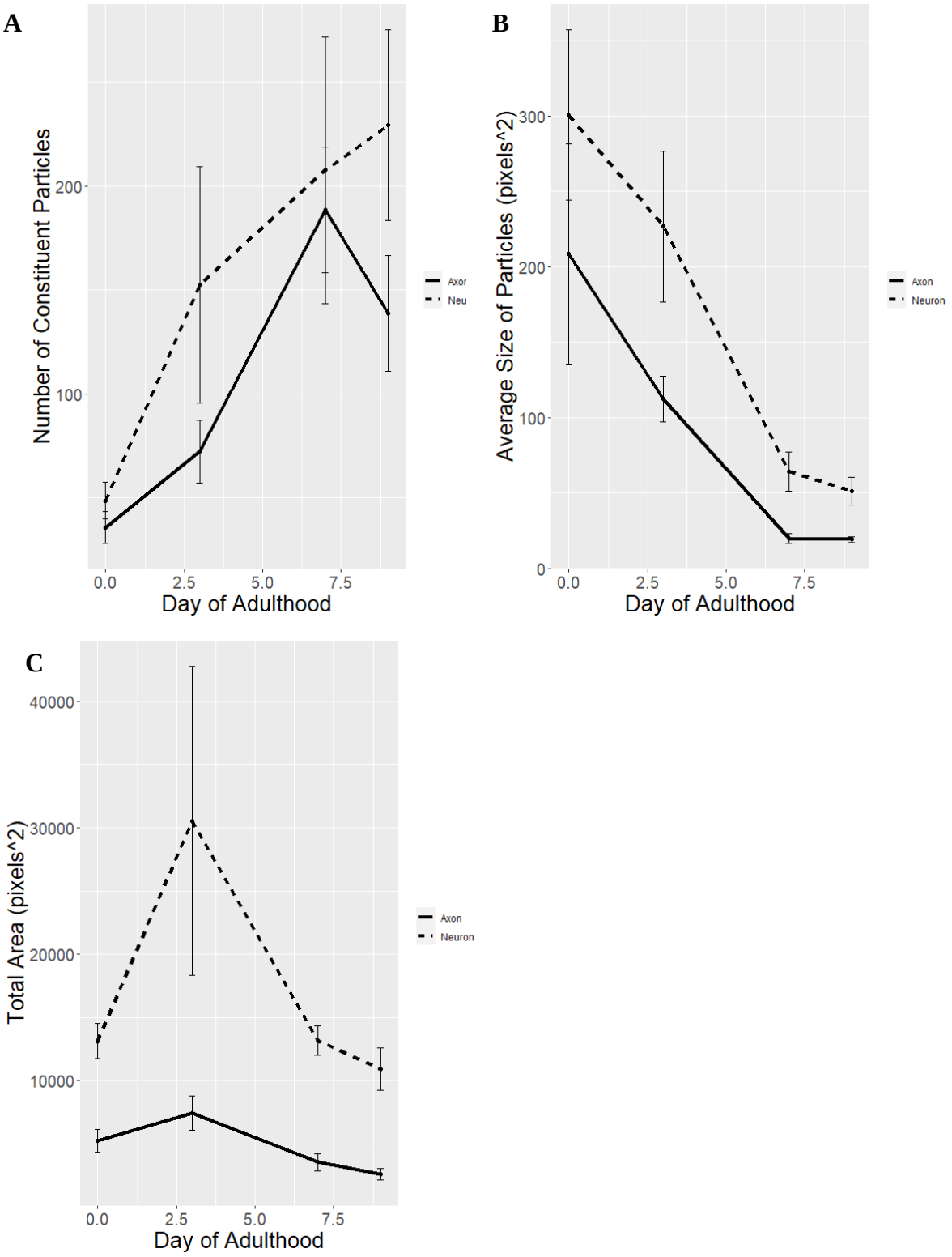

Figure 12. JVR168 neurodegeneration metrics (A) Number of constituent particles (B) Average size of particles (C) Total area

Figure 12 reports metrics of neurodegeneration over time in JVR168 worms carrying the human LRRK2::G2019S mutation. Panel A reflects a significant increase in particle count in both the axon ($p<0.001$) and axon + soma ($p=0.0336$) between larval stage 4 and adult day 9. A significant decrease in the average size of these particles was also observed in the axon ($p=0.00687$) and axon + soma ($p<0.001$), with a gradual decline between the L4 and A9 time-points (fig. 12B). While no significant differences were observed in the total area of the axon + soma ($p=0.135$), a significant increase in axonal area was observed between larval stage 4 and adult day 3 (fig. 12Cl). This was followed by a significant decline, approximately to the area of the L4 worms.

Discussion

Genotyping

A 1,010 base pair deletion noted the cat-2 gene of MT15620 worms is consistent with the known genotype of this strain. This deletion is associated with the loss of tyrosine-3-monooxygenase expression (Sawin et al. 2000; Yao et al. 2010; Omura et al. 2012). Necessary for dopamine synthesis, its loss is expected to impair dopaminergic functions including the basal slowing response.

N2 Basal Slowing Assay

The significant decreases in average speed and body lengths traveled per second between unseeded and seeded plates are indicative of an intact basal slowing response. These findings are consistent with those of Yao and colleagues in their 2010 study, which found significant decreases in average speed and body bends per second (not assayed in this experiment) in the presence of bacteria from adult day 0 to adult day 4. Omura and colleagues found that well fed wild type *C. elegans*, when in the presence of bacteria, moved at 76% of their speed on unseeded agar (Omura et al. 2012). Food deprived worms moved even slower, at 32% of their normal locomotor rate. Analysis of the N2 data from this work found that worms on seeded plates moved at 38% of the speed of those on an unseeded plate, which is in line with the data collected by Omura et al. Such results act as a positive control, verifying that this experimental protocol is capable of measuring the basal slowing response in *C. elegans*. However, it was also determined that maximum speed is not a useful indicator of the basal slowing response, as no significant difference was observed in N2 worms. With this knowledge, progression on to the evaluation of mutant worm strains was possible.

MT Basal Slowing Assay

The *C. elegans* strain MT15620 possesses a 1,010 bp deletion in the cat-2 gene, which is expected to produce a loss of dopaminergic behaviors including the basal slowing response (Sawin et. al 2000; Yao et al. 2010). Thus, it was hypothesized that these worms would exhibit no significant differences in body lengths per second (BLPS) and average speed between tracks generated in the presence or absence of a bacterial lawn. As such, they were intended to act as a negative control, indicating whether the loss of the basal slowing response is identifiable through the metrics recorded by WrmTrck. A complete and uniform loss of the basal slowing response across all life stages, as measured by both metrics, was not observed. The significant decrease in average speed of adult day 4 worms on seeded plates is consistent with an intact basal slowing response, as is the significant difference in body lengths per second. However, no significant differences in average speed or body lengths per second were noted in the L4s. This suggests that the basal slowing response was not present. An unexpected trend was observed with the average speed of adult day 7 worms, wherein the tracks generated on the seeded plate had a significantly greater average speed. This is an unusual reversal of the basal slowing response that has not been observed in any prior studies.

Unusual trends notwithstanding, the loss of the basal slowing response indicated by the L4 data indicates that this protocol can identify the loss of the basal slowing response. As such, the basal slowing assay facilitated by WrmTrck video analysis is a viable tool for quantifying *C. elegans* behavioral deficits.

However, the apparent recovery of the basal slowing response at adult day 4, as well as its reversal on day 7, defied expectations. These results are inconsistent with Yao et al. 2010, whose data demonstrated a complete absence of the basal slowing response across all life stages

in cat-2 mutant worms. It is worth noting that this study also demonstrated an interesting trend regarding speed of locomotion on a bacterial lawn, whereby baseline movement speed is affected by age. Regardless of strain or dopamine deficiency, *C. elegans* demonstrate an increase in movement speed from adult day 0 to adult day 2-3, followed by a sharp decline. However, their study did not report movement data on unseeded plates, thus it is unknown whether their worms followed the same trend in the absence of bacteria. The data from our longitudinal study of MT15620 worms is consistent with these findings, as adult day 4 worms exhibited the highest average and maximum speed on seeded agar. A study conducted by Omura and colleagues found that the movement speeds of cat-2 mutant *C. elegans* exhibited a wider variation than those of wildtype strains (Omura et al. 2012). However, this variation likely doesn't account for the statistically significant differences observed in this research. Repetition of this assay with a larger sample size would be useful to determine the normal phenotype of MT15620 worms with greater certainty.

JVR105 & JVR168 Basal Slowing Assay

The strain JVR105 was intended to act as a control for JVR168, as these worms express GFP in their dopaminergic neurons but not the time-dependent neurodegeneration associated with the human PD mutation. Thus, it was expected that they would display an intact basal slowing response like that of wildtype N2 worms. However, the data obtained in this study did not meet this expectation. On adult day 3, no significant differences in average speed or body lengths per second were observed between seeded and unseeded conditions. On adult day 7, worms on seeded plates exhibited significantly increased average speeds and body lengths per second on seeded compared to unseeded plates. This the opposite of the expected phenotype. There are two potential implications for this result: either the JVR105 worms are deficient in

their basal slowing response, or there is systematic error being introduced by the experimental apparatus. The former is highly unlikely, as JVR105 worms have demonstrated intact dopaminergic behaviors, including the basal slowing response, in prior studies (Maulik et al. 2017). Furthermore, data from fluorescent microscopy of these JVR105 worms were not indicative of significant damage or degeneration of the dopaminergic neurons. It is possible that an unknown developmental abnormality may exist within this worm stock, thus it would be advantageous to repeat the experiment with a new stock that arises from different progenitor worms. A systematic error may also be to blame for these abnormal results. However, since the positive (N2) and negative (MT15620) controls yielded results largely consistent with expectations, it is unlikely that a systematic error is to blame. Further study is needed to elucidate the cause of these unexpected results.

JVR168 worms expressing the human G2019S mutation represent the primary experimental group of this study, which sought to verify their phenotypes and potential for inclusion in a model system of PD. Prior research has demonstrated that LRRK2::G2019S worms exhibit time-dependent degradation of the basal slowing response, as well as degeneration of the dopaminergic neurons (Yao et al. 2010). The results of a basal slowing assay conducted on JVR168 worms were largely inconsistent with these expectations. Regardless of age, the worms did not exhibit an intact basal slowing response, as no significant slowing was observed on seeded plates. Yao and colleagues noted that day 0 adults demonstrated an intact basal slowing response, which was then found to be absent on day 2 and beyond. Adult day 3 and 7 worms in this study were found to lack a basal slowing response, consistent with the findings of Yao et al. Insignificant differences in both average speed and body lengths per second were observed on day 3, indicating that the worms were unable to sense and respond to

the bacterial lawn. A reversal of the basal slowing response was observed on adult day 7, wherein significant increases in speed and body lengths per second on seeded agar were noted. Though not the expected pattern, this is still indicative of impaired dopaminergic function and neurodegeneration.

Fluorescent Microscopy and DA Neuron Morphology Analysis

ImageJ was used to measure the average number of particles, average particle size, and total area of fluorescent dopaminergic neurons in both JVR105 and JVR168 *C. elegans*. JVR105 worms, expressing GFP but no known PD mutations, were not expected to display significant visual indicators of neurodegeneration (Maulik et al. 2017). Thus, this strain was employed as a control to identify natural changes in neuronal morphology across the *C. elegans* lifespan. A significant increase in total area between larval stage 4 and adult day 3 can likely be attributed to continued growth of the worms. No significant decreases in axonal or somatic average particle size were noted from larval stage 4 to adult day 9, which suggests that the neuron and axon are not undergoing degradation into smaller components. This lack of neurodegeneration is further supported by the insignificant change in particle count over time. This is consistent with the strain's known phenotype (Maulik et al. 2017). As such, it can be concluded that JVR105 is a useful control strain for the morphological examination of *C. elegans* neurons.

Neuronal morphology was evaluated in JVR168 worms to elucidate the relationship between neurodegeneration and deficits in dopaminergic behaviors. Because of their expression of the human LRRK2::G2019S mutation, it was expected that their dopaminergic neurons would exhibit a pattern of time-dependent degradation. The results of this study were found to be consistent with this prediction. A significant increase in particle count, as well as a corresponding decrease in average particle size, are indicative of neurodegeneration over time. This aligns with

the known phenotype of the JVR168 strain (Maulik et al 2017). However, total area did not appear to be a useful metric, as an insignificant overall change was noted between larval stage 4 and adult day 9. Similar results were also generated in a study conducted by Yao and colleagues, wherein they noted neuronal loss beginning on adult day 2 in all LRRK2 mutants tested (including G2019S) (2010). They also reported that this neurodegeneration worsened between days 5 and 9. We also noted such a trend, with the steepest increase in axonal particle count occurring between adult days 3 and 7 (72.4 particles to 189 particles).

Relationship of Basal Slowing Response and Neuronal Morphology

We intended to determine the relationship between dopaminergic neurodegeneration and behavioral deficits by correlating metrics of morphological change with the basal slowing response. Gaining an understanding of this interaction would add validity to our model system, providing redundant mechanisms with which to assess the effectiveness of potential therapeutic candidates. However, this was not possible due to the unexpected basal slowing assay results. Despite showing no evidence of morphological changes consistent with neuronal degradation, JVR105 worms did not exhibit an intact basal slowing response. As we were unable to obtain expected results from this control strain, we were unable to conclude that intact DA neurons are associated with intact dopaminergic behaviors.

Viability of Basal Slowing Assays as a Model System

Based on the results of this study, additional work is needed to evaluate the utility of the basal slowing assay as a disease model and drug screening tool. While expected results were demonstrated with positive (N2) and negative (MT15620) control strains, assays of JVR105 and JVR168 worms yielded data inconsistent with prior experiments. JVR105 worms, which express

no mutations affecting dopaminergic function and were expected to exhibit wildtype dopaminergic behaviors, had no demonstrable basal slowing response.

Future Work

In its current state, this assay is not a useful tool for evaluating behavioral deficits and dopaminergic dysfunction in *C. elegans.* Thus, future work largely centers around repetition and refinement of these experiments, with the goal of replicating the results of previously published studies. A starting point for this is expanding the sample size by increasing the number of worms tested, as well as the amount of footage collected. It may be of further benefit to also use new stocks of each worm strain, which would enable us to determine if the unexpected results in this study were observed because of genetic or developmental defects. Though unlikely, it is possible that systematic error was introduced by the microscope apparatus. Poor contrast and uneven focus in videos may have affected the ability of ImageJ to accurately track speed and distance. Thus, it may be beneficial to employ a higher-end microscope with higher image quality. The video analysis procedure used may have also introduced random or systematic error. Investigating the possibility of automating video analysis with ImageJ and WrmTrck has the potential to standardize the workflow and improve efficiency. Should these expansions and refinements yield more viable results, it would be possible to work towards replicating the work of others with known LRRK2 kinase inhibitors (Liu et al. 2011, Yao et al. 2012).

References

Azeggagh S, Berwick DC. 2021. The development of inhibitors of leucine-rich repeat kinase 2 (LRRK2) as a therapeutic strategy for Parkinson's disease: the current state of play. Br J Pharmacol.(bph.15575). doi:10.1111/bph.15575. http://dx.doi.org/10.1111/bph.15575

Beilina A, Bonet-Ponce L, Kumaran R, Kordich JJ, Ishida M, Mamais A, Kaganovich A, Saez-Atienzar S, Gershlick DC, Roosen DA, et al. 2020. The Parkinson's disease protein LRRK2 interacts with the GARP complex to promote retrograde transport to the trans-Golgi network. Cell Rep. 31(5):107614. doi:10.1016/j.celrep.2020.107614. http://dx.doi.org/10.1016/j.celrep.2020.107614.

Cooper JF, Van Raamsdonk JM. 2018. Modeling Parkinson's disease in C. elegans. J Parkinsons Dis. 8(1):17–32. doi:10.3233/JPD-171258. http://dx.doi.org/10.3233/JPD-171258.

Corsi AK, Wightman B, Chalfie M. 2015. A Transparent window into biology: A primer on Caenorhabditis elegans. WormBook.:1–31. doi:10.1895/wormbook.1.177.1. http://dx.doi.org/10.1895/wormbook.1.177.1.

Culetto E, Sattelle DB. 2000. A role for Caenorhabditis elegans in understanding the function and interactions of human disease genes. Hum Mol Genet. 9(6):869–877. doi:10.1093/hmg/9.6.869. http://dx.doi.org/10.1093/hmg/9.6.869.

Girault J-A, Greengard P. 2004. The neurobiology of dopamine signaling. Arch Neurol. 61(5):641–644. doi:10.1001/archneur.61.5.641. http://dx.doi.org/10.1001/archneur.61.5.641.

Goldman SM, Marek K, Ottman R, Meng C, Comyns K, Chan P, Ma J, Marras C, Langston JW, Ross GW, et al. 2019. Concordance for Parkinson's disease in twins: A 20-year update. Ann Neurol. 85(4):600–605. doi:10.1002/ana.25441. http://dx.doi.org/10.1002/ana.25441.

Jankovic J. 2008. Parkinson's disease: clinical features and diagnosis. J Neurol Neurosurg Psychiatry. 79(4):368–376. doi:10.1136/jnnp.2007.131045. http://dx.doi.org/10.1136/jnnp.2007.131045.

Kneynsberg A, Collier TJ, Manfredsson FP, Kanaan NM. 2016. Quantitative and semi-quantitative measurements of axonal degeneration in tissue and primary neuron cultures. J Neurosci Methods. 266:32–41. doi:10.1016/j.jneumeth.2016.03.004. http://dx.doi.org/10.1016/j.jneumeth.2016.03.004.

Konnova EA, Translational Neurogenetics Unit, Wallenberg Neuroscience Center, Lund University, Lund, Sweden, Swanberg M, Translational Neurogenetics Unit, Wallenberg Neuroscience Center, Lund University, Lund, Sweden. 2018. Animal

models of Parkinson's disease. In: Parkinson's Disease: Pathogenesis and Clinical Aspects. Codon Publications. p. 83–106.

Lanciego JL, Luquin N, Obeso JA. 2012. Functional neuroanatomy of the basal ganglia. Cold Spring Harb Perspect Med. 2(12):a009621. doi:10.1101/cshperspect.a009621. http://dx.doi.org/10.1101/cshperspect.a009621.

Leonard N, Vidal-Gadea AG. 2021. Affordable Caenorhabditis elegans tracking system for classroom use. bioRxiv. doi:10.1101/2020.12.28.424585. http://dx.doi.org/10.1101/2020.12.28.424585.

Liu Z, Hamamichi S, Lee BD, Yang D, Ray A, Caldwell GA, Caldwell KA, Dawson TM, SmithW, Dawson VL. 2011. Inhibitors of LRRK2 kinase attenuate neurodegeneration and Parkinson-like phenotypes in C. elegans and Drosophila Parkinson's disease models. Human Molecular Genetics. 20(20):3933–3942.

Madureira M, Connor-Robson N, Wade-Martins R. 2020. LRRK2: Autophagy and lysosomal activity. Front Neurosci. 14:498. doi:10.3389/fnins.2020.00498. http://dx.doi.org/10.3389/fnins.2020.00498.

Maulik M, Mitra S, Bult-Ito A, Taylor BE, Vayndorf EM. 2017. Behavioral phenotyping and pathological indicators of Parkinson's disease in C. elegans models. Front Genet. 8. doi:10.3389/fgene.2017.00077. http://dx.doi.org/10.3389/fgene.2017.00077.

Mody S. 2021. The Search for Reliable Behavioral Assays to Model Parkinson's Disease in the Nematode Caenorhabditis elegan. [Madison NJ]: Drew University.

Omura DT, Clark DA, Samuel ADT, Horvitz HR. 2012. Dopamine signaling is essential for precise rates of locomotion by C. elegans. PLoS One. 7(6):e38649. doi:10.1371/journal.pone.0038649. http://dx.doi.org/10.1371/journal.pone.0038649.

Poewe W, Seppi K, Tanner CM, Halliday GM, Brundin P, Volkmann J, Schrag A-E, Lang AE. 2017. Parkinson disease. Nat Rev Dis Primers. 3(1):17014. doi:10.1038/nrdp.2017.14. http://dx.doi.org/10.1038/nrdp.2017.14.

Sawin ER, Ranganathan R, Horvitz HR. 2000 C. elegans Locomotory Rate is Modulated by the Environment through a Dopaminergic Pathway and by Experience through a Serotonergic Pathway. Neuron. 26(3):619–631.

Simon DK, Tanner CM, Brundin P. 2020. Parkinson disease epidemiology, pathology, genetics, and pathophysiology. Clin Geriatr Med. 36(1):1–12. doi:10.1016/j.cger.2019.08.002. http://dx.doi.org/10.1016/j.cger.2019.08.002.

Usmani A, Shavarebi F, Hiniker A. 2021. The cell biology of LRRK2 in Parkinson's disease. Mol Cell Biol. 41(5). doi:10.1128/MCB.00660-20. http://dx.doi.org/10.1128/MCB.00660-20.

West AB, Moore DJ, Choi C, Andrabi SA, Li X, Dikeman D, Biskup S, Zhang Z, Lim K-L, Dawson VL, et al. 2007. Parkinson's disease-associated mutations in LRRK2 link enhanced GTP-binding and kinase activities to neuronal toxicity. Hum Mol Genet. 16(2):223–232. doi:10.1093/hmg/ddl471. http://dx.doi.org/10.1093/hmg/ddl471.

White JG, Southgate E, Thomson JN, Brenner S. 1986. The structure of the nervous system of the nematode Caenorhabditis elegans. Philos Trans R Soc Lond B Biol Sci. 314(1165):1–340. doi:10.1098/rstb.1986.0056. http://dx.doi.org/10.1098/rstb.1986.0056.

Yao C, El Khoury R, Wang W, Byrd TA, Pehek EA, Thacker C, Zhu X, Smith MA, Wilson-Delfosse AL, Chen SG. 2010. LRRK2-mediated neurodegeneration and dysfunction of dopaminergic neurons in a Caenorhabditis elegans model of Parkinson's disease. Neurobiol Dis. 40(1):73–81. doi:10.1016/j.nbd.2010.04.002. http://dx.doi.org/10.1016/j.nbd.2010.04.002.

Yao C, Johnson WM, Gao Y, Wang W, Zhang J, Deak M, Alessi DR, Zhu X, Mieyal JJ, Roder H, et al. 2013. Kinase inhibitors arrest neurodegeneration in cell and C. elegans models of LRRK2 toxicity. Hum Mol Genet. 22(2):328–344. doi:10.1093/hmg/dds431. http://dx.doi.org/10.1093/hmg/dds431.